IEEE Access
Multidisciplinary ⋮ Rapid Review ⋮ Open Access Journal

Received July 18, 2021, accepted August 11, 2021, date of publication August 17, 2021, date of current version August 26, 2021.

Digital Object Identifier 10.1109/ACCESS.2021.3105608

Quantitative Comparison of Power Densities Related to Electromagnetic Near-Field Exposures With Safety Guidelines From 6 to 100 GHz

KUN LI[1,2], (Member, IEEE), KENSUKE SASAKI[2], (Member, IEEE), KANAKO WAKE[2], (Member, IEEE), TERUO ONISHI[2], (Member, IEEE), AND SOICHI WATANABE[2], (Senior Member, IEEE)

[1]Faculty of Engineering and Design, Kagawa University, Takamatsu, Kagawa 761-0396, Japan
[2]National Institute of Information and Communications Technology, Koganei, Tokyo 184-8795, Japan

Corresponding author: Kun Li (li.kun@kagawa-u.ac.jp)

This work was supported in part by the Ministry of Internal Affairs and Communications of Japan under Grant JPMI10001.

ABSTRACT This paper presents a quantitative analysis of the differences between the various definitions of spatially averaged power densities ($sIPD_s$) for localized exposure to electromagnetic near-fields at frequencies from 6 to 100 GHz. The spatially averaged modulus of the complex Poynting vector ($sIPD_{mod}$) and spatially averaged norm of the real part of the complex Poynting vector ($sIPD_{norm}$) were compared using numerical approaches, where their relationships with the spatially averaged absorbed power density ($sAPD$) and the local peak temperature elevation on skin tissue were analyzed. Our results demonstrated that outside the typical boundary of the reactive near-field, i.e., $> \lambda/(2\pi)$, which is used as a rough guide of the applicable condition for reference levels in the RF safety guidelines, but at most 10 mm from the radiation source, the maximum difference between $sIPD_{norm}$ and $sIPD_{mod}$ is smaller than 0.7 dB from 6 to 100 GHz. For the appropriate conditions recommended in the RF safety guidelines, the differences between the ratios of $sAPD$ to $sIPD_s$ and those for the plane-wave normal incidence, are at most 1.4 dB and 0.9 dB for $sIPD_{norm}$ and $sIPD_{mod}$, respectively. Under the same condition, the ratios of the temperature rise to $sIPD_s$ for the relatively small antennas (total dimension less than 2λ) do not significantly exceed that for the plane-wave normal incidence, which means that the expected maximum temperature rise is lower than the temperature rise that is derived from the operational health effect threshold in terms of the temperature rise divided with the reduction factors employed in the RF safety guidelines. The above results provide suggestive evidence that the effect of the definition of $sIPD_s$ on the human exposure characteristics is not significant compared with those of the other factors, i.e., the antenna type (size), frequency, distance from the source, and averaging area.

INDEX TERMS Electromagnetic fields, dosimetry, radiation safety, near-field, power density, temperature elevation, millimeter wave.

I. INTRODUCTION

The rapid increase in the use of radio frequency (RF) transmitters in millimeter wave (MMW) bands has raised public concerns regarding human exposure to electromagnetic fields (EMFs) in a general living environment [1]–[3]. Localized temperature elevation on the human skin surface due to MMW exposure is recognized as a dominant cause of adverse health effects [4]–[6]. Safety guidelines and standards have prescribed the limits for EMF exposure to prevent excessive temperature elevation on human tissues in the frequency range from 6 to 300 GHz. The International Commission on Non-Ionizing Radiation Protection (ICNIRP-2020 safety guidelines) [7] defined absorbed power density (APD) as a new metric for the basic restrictions to protect against the adverse health effects associated with superficial heating due to localized exposure. Similarly, IEEE Std C95.1 [8] specified epithelial power density as the

The associate editor coordinating the review of this manuscript and approving it for publication was Zhengqing Yun.

metric of dosimetric reference limits (DRLs) in the frequency band.

Because the basic restrictions/DRLs are related to physical quantities inside an exposed body, which cannot be easily measured, the reference level/exposure reference levels (ERLs) have been used in the ICNIRP-2020 safety guidelines [7] and IEEE Std C95.1 [8], respectively, to serve as practical measures for safety compliance assessment [9]. In the case of local exposure for a period exceeding 6 minutes, the spatially averaged incident power density (*IPD*) is utilized as the metric of the reference levels/ERLs at frequencies over 6 GHz. The reference levels/ERLs of *IPD* for local exposure are frequency-dependent values of $275f_G^{-0.177}$ and $55f_G^{-0.177}$ (W/m^2) (f_G: frequency in GHz) from 6 to 300 GHz for occupational exposure/restricted environments and general public exposure/unrestricted environments, respectively (ICNIRP-2020 safety guidelines [7], IEEE Std C95.1 [8]).

In the ICNIRP-2020 safety guidelines [7], it is recommended that *APD* is averaged over an area of 4 cm^2 from 6 to 300 GHz as a practical protection specification owing to its good correlation with the local maximum temperature elevation. Furthermore, for frequencies ranging from 30 to 300 GHz, it is recommended that the spatial average is reduced to approximately 1 cm^2 to account for the possibility of smaller beam exposure scenarios, where an additional constraint (twice that of 4 cm^2) should be imposed. For consistency with the basic restrictions/DRLs, the same averaging areas of the reference levels/ERLs are employed [7], [8].

To explain the relationship between the power densities and the resultant surface temperature elevation at MMW bands, dosimetric studies for plane-wave exposures were conducted [10]–[15]. IPD_s values from RF wireless devices over 6 GHz, such as prototypes of 5G mobile antennas, have been studied in [16]–[24]. [18] and [24] reported research results including those under beam steering exposure conditions at 28 GHz, i.e., the FR2 (MMW) frequency band assigned in Japan and some other countries. These studies investigated the appropriate definitions for spatially averaged IPD_s at 28 GHz, but the related discussions have not yet been extended to other frequency bands from 6 to 300 GHz.

For the compliance assessments of RF wireless devices at MMW bands, the IEC Technical Committee (TC) 106 and IEEE ICES TC34 considered the norm or normal components of the real part of the complex Poynting vector as metrics for practical near-field compliance. The comparison of these two definitions is being discussed in working groups under IEEE ICES TC95. On the other hand, the ICNIRP [7] defined *IPD* as the modulus of the complex Poynting vector, which includes both the real and imaginary components. This may be in consideration of the requirements associated with the determination of more conservative exposure limits for near-field exposure situations in the safety guidelines, because the imaginary component of the complex Poynting vector will be gradually increased as the distance from the antenna decreases to less than the reactive near-field boundary. Christ *et al.* [25] discussed the impact on the aforementioned IPD_s to explain the effect of the reactive near-field using typical antennas at 1, 10, and 30 GHz. However, the relationships between the power densities and the resultant skin temperature elevation were not fully discussed in [25]. Therefore, this research attempts to investigate which of the two IPD_s, namely, the modulus of the complex Poynting vector and the norm of the real part of the complex Poynting vector, is better correlated with the skin surface temperature elevation under antenna near-field exposure conditions.

In this study, we investigated the differences due to the definitions of the incident power density in detail. In particular, the relationships between each definition of the spatially averaged power density and skin temperature elevation were compared using computational approaches for different antennas and exposure conditions at frequencies from 6 to 100 GHz. Because the ICNIRP [7] specifies that the reference levels in terms of *IPD* are not applicable within the reactive near-field, the main purpose of this study was to understand the applicability of these two spatially averaged IPD_s when approaching the boundary between the reactive and radiative antenna near-fields.

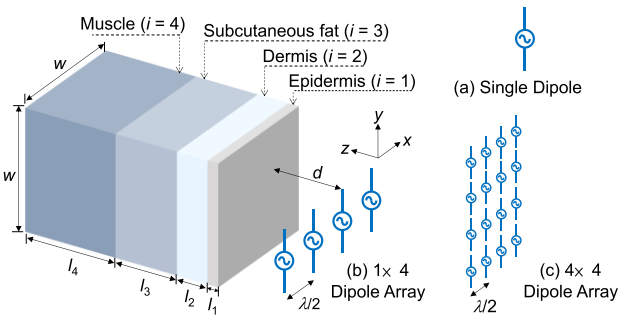

FIGURE 1. Computational model: a three-dimensional four-layer skin model comprised of epidermis ($i = 1$), dermis ($i = 2$), subcutaneous fat ($i = 3$), and muscle ($i = 4$) exposed to vertically polarized antennas, (a) single dipole, (b) 1 × 4 dipole array, and (c) 4 × 4 dipole array.

II. ANALYTICAL MODEL AND METHOD

A. CONFIGURATION OF MULTI-LAYER HUMAN SKIN MODEL

Fig. 1 illustrates a computational model for dosimetry analysis. A four-layer tissue model, which is composed of epidermis ($i = 1$), dermis ($i = 2$), subcutaneous fat ($i = 3$), and muscle ($i = 4$), was used to represent the skin tissue configuration in the forearm [13], [14]. The width w of the skin model and thickness of each layer, l_i, are listed in Table 1. It is known that the model size used in this study is sufficiently large for temperature analysis [18]. The dielectric properties reported in [13], [26] were used.

For an electromagnetic near-field radiation source, single half-wavelength vertical dipole, 1 × 4 dipole array, and 4 × 4 dipole array antennas comprising half-wavelength dipoles with in-phase excitations at frequencies from 6 to 100 GHz

were employed, as shown in Figs. 1 (a), (b), and (c), respectively. Each antenna was placed parallel to the surface of the skin model with vertical polarization. The separation distance from the skin surface to the antenna element was set to d (mm). In each scenario with and without skin model, the total antenna input power was normalized to an identical value.

The finite-difference time-domain (FDTD) method [27]–[32] was used to analyze the EMFs both outside and inside the skin model. The computational region was truncated by 10-layer Berenger's perfectly matched layer boundaries.

TABLE 1. Dimensions of the four-layer skin model for dosimetry computations.

Model size (mm)	Frequency (GHz)		
	6–30	40–60	100
w	100	50	25
l_1	0.2	0.2	0.2
l_2	1.0	1.0	1.0
l_3	3.8	3.8	3.8
l_4	15	15	5.0
Resolution (mm)	0.2	0.1	0.05

TABLE 2. Parameters used in temperature elevation computations.

Parameters	Epidermis ($i = 1$)	Dermis ($i = 2$)	Subcutaneous fat ($i = 3$)	Muscle ($i = 4$)
κ (W/(m°C))	0.42	0.42	0.25	0.50
ρ (kg/m^3)	1109	1109	911	1090
c (J/(kg °C))	3600	3600	3000	3800
M_i (W/m^3)	1620	1620	300	480
B_i (W/(m°C))	0	9100	1700	2700

B. THERMAL PARAMETERS AND COMPUTATION

The temperature elevation in the steady state due to EMF exposure can be obtained by solving the Pennes bioheat transfer equation [29]–[37] as follows:

$$c(\boldsymbol{r})\,\rho(\boldsymbol{r})\,\frac{\partial T(\boldsymbol{r},t)}{\partial t} = \nabla\cdot(\kappa(\boldsymbol{r})\cdot\nabla T(\boldsymbol{r},t)) + \rho(\boldsymbol{r})\,\mathrm{SAR}(\boldsymbol{r}) + M(\boldsymbol{r},t) - B(\boldsymbol{r},t)\,(T(\boldsymbol{r},t) - T_b(\boldsymbol{r},t)), \quad (1)$$

where T and T_b are the temperatures of the human tissues and blood (°C), respectively. c is the specific heat (J/(kg°C)), and κ is the thermal conductivity (W/(m°C)). t is the time variable. M is the basal metabolism per unit volume (W/m^3) and B is a term associated with the blood flow in each skin tissue (W/(m^3°C)). The specific absorption rate (SAR) (W/kg), which represents the heat-generating source related to electromagnetic wave exposure [17], [29], [38], is defined as

$$\mathrm{SAR}(\boldsymbol{r}) = \sigma(\boldsymbol{r})\,\frac{|\boldsymbol{E}(\boldsymbol{r})|^2}{2\rho(\boldsymbol{r})}, \quad (2)$$

where $|\boldsymbol{E}(\boldsymbol{r})|$ is the amplitude of the induced electric field inside the skin tissue and $\boldsymbol{r}$ denotes the position vector. σ and ρ are the electrical conductivity (S/m) and mass density (kg/m^3), respectively. The boundary condition for the heat exchange between the air and skin tissue is given as

$$-\kappa(\boldsymbol{r})\,\frac{\partial T(\boldsymbol{r},t)}{\partial \boldsymbol{n}} = h\left(T_{surf}(\boldsymbol{r},t) - T_{air}(t)\right), \quad (3)$$

where h, T_{surf}, and T_{air} denote the heat transfer coefficient (W/(m°C)), the temperature of the skin surface tissue, and that of the air, respectively. $\boldsymbol{n}$ is the normal unit vector component that represents the boundary surface.

To ensure consistency with previous works [13], [14], [39], similar parameters were used for the thermal analysis, which are listed in Table 2. The heat transfer coefficient h between the air and skin surface was set to 10 W/(m°C). The temperature at the end of the muscle was fixed at the body core temperature of 37 °C and the air temperature was 20 °C. All the other boundary conditions were set to be adiabatic.

C. SPATIALLY AVERAGED INCIDENT AND ABSORBED POWER DENSITIES

For the compliance assessment of mobile terminals such as smartphones that are used in close proximity to a human body above 6 GHz, a method for evaluating $sIPD_s$ at the evaluation surface with a separation distance greater than or equal to 2 mm from any part of the device has been provided [9]. In antenna theory [40], for a short dipole antenna or an equivalent radiator, the typical boundary between the reactive and radiative near-fields is commonly considered to exist at a distance of $\lambda/(2\pi)$ (λ: free space wavelength) from the antenna surface. Therefore, $\lambda/(2\pi)$ is used as a rough guide to find the approximate boundary between the reactive and radiative antenna near-fields [7]. According to this consideration, the outer boundary can be expected to be from 8 to 0.16 mm at frequencies from 6 to 300 GHz. This suggests that at the minimum distance (2 mm) for the compliance test of a wireless device, it is possible to enter the range of the reactive near-field up to 24 GHz. Therefore, $sIPD_s$ in the antenna near-field should be carefully handled to prevent excessive EMF exposures.

The two $sIPD_s$ used in this study are defined in the safety guidelines and standards, i.e., the spatially averaged value of the modulus of the complex Poynting vector ($sIPD_{mod}$) and the norm of the real part of the complex Poynting vector ($sIPD_{norm}$), as shown below:

$$sIPD_{mod}(\boldsymbol{r}) = \frac{1}{2A}\iint_A \left\|\boldsymbol{E}(\boldsymbol{r})\times\boldsymbol{H}^*(\boldsymbol{r})\right\| dA, \quad (4)$$

$$sIPD_{norm}(\boldsymbol{r}) = \frac{1}{2A}\iint_A \left|\mathrm{Re}\left(\boldsymbol{E}(\boldsymbol{r})\times\boldsymbol{H}^*(\boldsymbol{r})\right)\right| dA, \quad (5)$$

where $\mathbf{E}$ and $\mathbf{H}^*$ denote the electric field phasor and the complex conjugate of the magnetic field phasor, respectively. The symbol A indicates the spatial average area. Eq. (4) includes all components of the complex Poynting vector with both real and imaginary parts, which is used in the ICNIRP-2020 safety guidelines [7]. Eq. (5) employs the real part of the complex Poynting vector crossing a surface of interest, as denoted by [24]. In this study, Eqs. (4) and (5) were adopted to compare their correlations with the absorbed power density and with the temperature elevation resulting from exposure to the antennas under various near-field exposure conditions.

The spatially averaged absorbed power density (*sAPD*) crossing an area in the air to skin boundary in the direction normal to the interface represents the total power absorbed by the skin tissue [41], [42], which is expressed by the following equation, as proposed in the ICNIRP-2020 safety guidelines [7]:

$$sAPD\,(\boldsymbol{r}) = \iint_A \mathrm{Re}\left(\boldsymbol{E}\,(\boldsymbol{r}) \times \boldsymbol{H}^*\,(\boldsymbol{r})\right) \cdot d\boldsymbol{s}/A, \qquad (6)$$

where $d\boldsymbol{s}$ denotes the integral variable vector whose direction is normal to the integral area A on the body surface, as shown in the coordinate of Fig. 1. Note that *sAPD* in Eq. (6) was averaged over the square surface area of the skin model shown in Fig. 1. The $sIPD_s$ values in Eqs. (4) and (5) were averaged over a square in free space to which the body surface space is projected [7], with the same dimension as that of the *sAPD*.

III. RESULTS

A. COMPARISON OF INCIDENT POWER DENSITIES IN ANTENNA NEAR-FIELD WITHOUT HUMAN BODY

Fig. 2 shows the ratio of $sIPD_{norm}$ to $sIPD_{mod}$ as a function of the separation distance d from antenna surface normalized with the wavelength λ in free space. The data at each frequency were calculated with d increased from 2 to 10 mm at 1 mm intervals. The spatial averaging area A of $sIPD_s$ was set to 4 and 1 cm^2, as shown in Figs. 2 (a) and (b), respectively.

In this section, emphasis is placed on the condition that $sIPD_{norm}/sIPD_{mod}$ is much less than 0 dB, which results in the possible underestimation of the exposure level when $sIPD_{norm}$ is employed for compliance evaluation with the RF safety guidelines. For convenience, the condition of $sIPD_{norm}/sIPD_{mod}$ of -1 dB or less is examined as a measure. The reason is that considering the uncertainty of the evaluation, the discussion of minute differences (numerical values near 0 dB) lacks scientific validity. In addition, a 1 dB absolute difference may not be negligible for the reduction factor of 2 (about 3 dB) that was used for deriving the basic restrictions from the operational health effect threshold in local exposure above 6 GHz in the ICNIRP-2020 safety guidelines

1) DEPENDENCE ON EXPOSURE CONDITIONS

As shown in Fig. 2, the difference between $sIPD_{norm}$ and $sIPD_{mod}$ increases monotonically with decreasing separation distance d. Many results of $sIPD_{norm}/sIPD_{mod}$ are lower than -1 dB when the distance d is shorter than the typical reactive and radiative near-field boundary, i.e., $d < \lambda/(2\pi)$. This is because the contribution from the imaginary component of the complex Poynting vector increases markedly in the antenna reactive near-field.

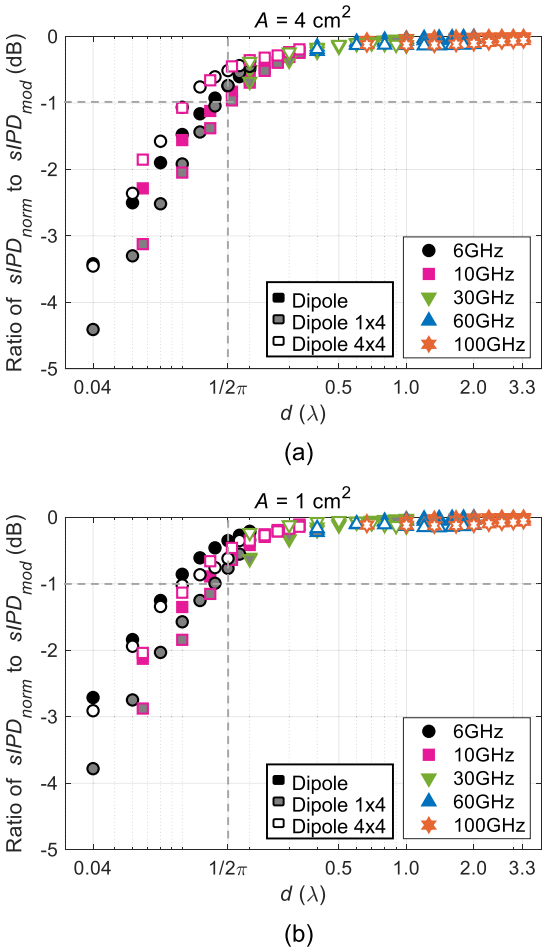

FIGURE 2. Ratio of $sIPD_{norm}$ to $sIPD_{mod}$ for the single dipole, 1 × 4 dipole array, and 4 × 4 dipole array antennas as a function of the antenna–skin separation distance d from 2 to 10 mm, normalized with the wavelength λ, at frequencies of 6, 10, 30, 60, and 100 GHz. $sIPD_S$ values are averaged over square areas of (a) $A = 4$ cm^2 and (b) $A = 1$ cm^2.

On the other hand, the difference between $sIPD_{norm}$ and $sIPD_{mod}$ monotonically approaches 0 dB with increasing d. At separation distances of $d > \lambda/(2\pi)$, $sIPD_{norm}/sIPD_{mod}$ is always within -1 dB.

For the separation distances ($d \geq 2$ mm) and antenna types considered in this study, $sIPD_{norm}/sIPD_{mod} < -1$ dB is only found in several cases of 6 and 10 GHz. Above 30 GHz, the results of $sIPD_{norm}/sIPD_{mod}$ are within -1 dB in all cases.

Moreover, at $d < \lambda/(2\pi)$, the maximum variation caused by the different antenna types is 1.3 and 1.1 dB when $A = 4$ and 1 cm^2, respectively. At separation distances of $d > \lambda/(2\pi)$, the corresponding variations reduce to 0.4 and 0.5 dB, respectively.

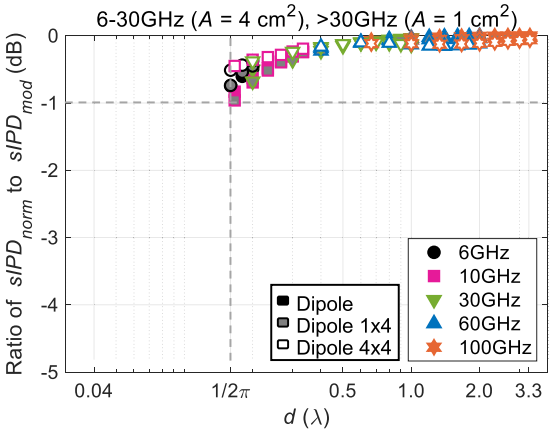

FIGURE 3. Ratio of $sIPD_{norm}$ to $sIPD_{mod}$ for the single dipole and dipole array antennas as a function of the antenna–skin separation distance d from $\lambda/(2\pi)$ to 10 mm at frequencies from 6 to 100 GHz averaged over square areas of $A = 4$ and 1 cm^2 at or below 30 GHz and above 30 GHz, respectively.

These results indicate that at the distances ($d \geq 2$ mm) and frequencies (6 to 100 GHz) assumed in this study, there is no large difference in the dependence on the antenna type for the condition that $sIPD_{norm}/sIPD_{mod} < -1$ dB.

2) DEPENDENCE ON EXPOSURE ASSESSMENT METHOD

When the different spatial averaging areas of 4 and 1 cm^2 were used, as respectively shown in Figs. 2 (a) and (b), the maximum variation between $sIPD_{norm}$ and $sIPD_{mod}$ was within 0.7 dB for the case of the single dipole at 6 GHz when $d = 2$ mm. At $d > \lambda/(2\pi)$, this difference changed to 0.4, 0.3, and 0.1 dB in the cases of the single dipole, 1×4 dipole array, and 4×4 dipole array, respectively, but slightly increased up to 0.7, 0.6, and 0.5 dB, respectively, at $d < \lambda/(2\pi)$.

Although the above-mentioned data show that the dependence on the spatial averaging area is relatively large in the antenna near-field, this conclusion is not very clear since the variation is still within 1 dB. Therefore, under the assumptions of the distance ($d \geq 2$ mm) and frequency (6 to 100 GHz) in this study, it can be considered that there is no marked difference in the dependence on the spatial averaging area for the condition that $sIPD_{norm}/sIPD_{mod} < -1$ dB.

3) WORST CASE

From Fig. 2, it can be found that the lowest values of $sIPD_{norm}/sIPD_{mod}$ under all conditions are -4.4 and -3.8 dB when $A = 4$ and 1 cm^2, respectively, which are much lower than -1 dB. The worst condition occurs in the case of the 1×4 dipole array at 6 GHz when $d = 2$ mm.

On the other hand, Fig. 3 shows the ratio of $sIPD_{norm}$ to $sIPD_{mod}$ as a function of the separation distance d when the conditions of $sIPD_s$ specified in the ICNIRP-2020 safety guidelines were employed ($d \geq \lambda/(2\pi)$, $A = 4$ cm^2 at 6–30 GHz, whereas $A = 1$ cm^2 over 30 GHz). In Fig. 3, it is shown that the lowest value of $sIPD_{norm}/sIPD_{mod}$ under the applicable conditions of the ICNIRP-2020 safety guidelines is within -1 dB. The worst case of -1 dB is found at $d = 5$ mm when using the 1×4 dipole array at 10 GHz.

B. COMPARISON OF POWER TRANSMISSION FOR NEAR-FIELD EXPOSURES

Figs. 4 and 5 show the ratio of *sAPD* to *sIPD*, i.e., the power transmission, normalized with that of a plane-wave normal incidence condition [14] as a function of the antenna to skin separation distance (d) normalized with λ at frequencies from 6 to 100 GHz. Similar to the condition in Fig. 2, the single dipole, 1×4 dipole array, and 4×4 dipole array antennas were considered. The square areas A for spatial averaging of 4 and 1 cm^2 are applied in Figs. 4 and 5, respectively. In this section, we focus on the condition that the normalized *sAPD*/*sIPD* is much greater than 0 dB. For similar reasons to those mentioned in Sec. III. A, a deviation of 1 dB or more is considered as a measure here.

1) DEPENDENCE ON EXPOSURE CONDITIONS

As shown in Figs. 4 and 5, the results of $sAPD/sIPD_{norm}$ and $sAPD/sIPD_{mod}$ normalized with those of plane-wave incidence increases markedly when $d < \lambda/(2\pi)$, where for many cases, the deviations significantly exceed 0 dB (> 1 dB). Even when $d > \lambda/(2\pi)$, as shown in Figs. 4 and 5, depending on the exposure conditions (antenna type, frequency) and exposure evaluation methods (*sIPD* definition, averaging area), the normalized *sAPD*/*sIPD* still exceeds 1 dB in several cases.

Moreover, *sAPD*/*sIPD* normalized with the plane-wave incidence increases with decreasing frequency. At frequencies of 6 and 10 GHz, the normalized *sAPD*/*sIPD* may significantly exceed 0 dB (> 1 dB). At 30 GHz and above, on the other hand, the corresponding results do not significantly exceed 0 dB.

Furthermore, as shown in Figs. 4 and 5, we observed that there is no significant discrepancy in the dependence on the antenna type under the condition that the normalized *sAPD*/*sIPD* significantly exceeds 0 dB (> 1 dB) as considered in this section.

From Figs. 4 and 5, at $d < \lambda/(2\pi)$, the variation in the normalized *sAPD*/*sIPD* with the antenna type is relatively small (< 2 dB) compared with the variations due to the antenna–skin separation distance and frequency. When $d > \lambda/(2\pi)$, on the other hand, the difference in the normalized *sAPD*/*sIPD* more strongly depends on the antenna type (up to 5 dB or more).

2) DEPENDENCE ON EXPOSURE ASSESSMENT METHOD

In Figs. 4 and 5, it is shown that there is no marked difference in the conditions under which the normalized *sAPD*/*sIPD* significantly exceeds 0 dB (> 1 dB) between the definitions of the incident power density. The normalized $sAPD/sIPD_{norm}$ from plane-wave normal incidence is slightly higher than that of $sAPD/sIPD_{mod}$. At $d < \lambda/(2\pi)$, the variation in the normalized *sAPD*/*sIPD* due to the difference in the definition of *sIPD* is relatively large (up to 3 to 4 dB). When the

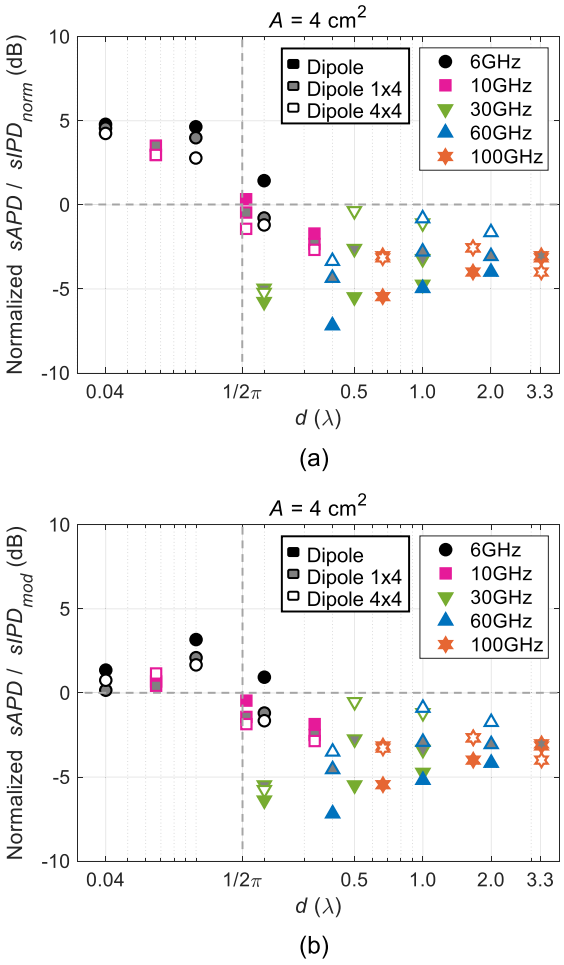

FIGURE 4. Ratios of spatially averaged absorbed to incident power densities for the dipole and dipole array antennas at frequencies from 6 to 100 GHz. The ratios are normalized with those of plane-wave normal incidence. The antenna–skin separation distances d of 2, 5, and 10 mm are normalized with the wavelength at each frequency. The averaging area is $A = 4$ cm^2: (a) $sAPD/sIPD_{norm}$, (b) $sAPD/sIPD_{mod}$.

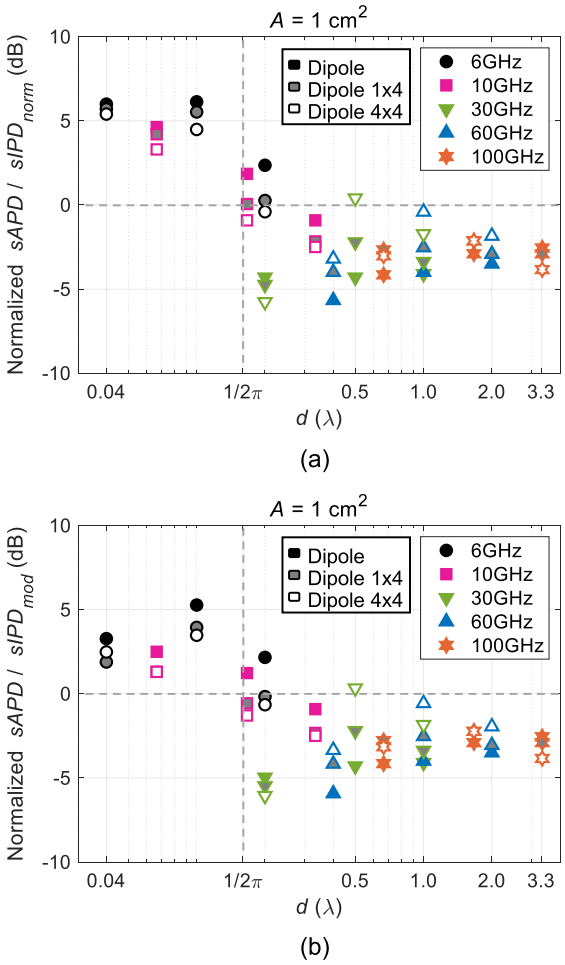

FIGURE 5. Ratios of spatially averaged absorbed to incident power densities for the dipole and dipole array antennas at frequencies from 6 to 100 GHz. The ratios are normalized with those of plane-wave normal incidence. The antenna–skin separation distances d of 2, 5, and 10 mm are normalized with the wavelength at each frequency. The averaging area is $A = 1$ cm^2: (a) $sAPD/sIPD_{norm}$, (b) $sAPD/sIPD_{mod}$.

separation distance $d > \lambda/(2\pi)$, the corresponding variation reduces to less than 1 dB.

On the other hand, there is no obvious difference in the conditions under which the normalized $sAPD/sIPD$ significantly exceeds 0 dB (> 1 dB) between the spatial averaging areas.

3) WORST CASE

The ratio of $sAPD$ to $sIPD$ as a function of the separation distance d under the applicable conditions of $sIPD_s$ specified in the ICNIRP-2020 safety guidelines ($d \geq \lambda/(2\pi)$, $A = 4$ cm^2 at 6–30 GHz, whereas $A = 1$ cm^2 over 30 GHz) is shown in Fig. 6. In Fig. 6, the highest deviations of the normalized $sAPD/sIPD$ under all the conditions are over 3 to 6 dB, which significantly exceed 0 dB (> 1 dB).

Considering the conditions of $sIPD_s$ specified in the ICNIRP-2020 safety guidelines ($d \geq \lambda/(2\pi)$, $A = 4$ cm^2 at 6–30 GHz, whereas $A = 1$ cm^2 over 30 GHz), as shown in Fig. 6, the highest deviations of the normalized $sAPD/sIPD_{norm}$ in comparison with that under plane-wave exposure slightly exceed 0 dB (at most 1.4 dB). For the case of the normalized $sAPD/sIPD_{mod}$, the highest deviations do not significantly exceed 0 dB (at most 0.9 dB).

C. COMPARISON OF HEATING FACTORS FOR NEAR-FIELD EXPOSURES

Considering the impact of the definitions of $sIPD_s$ on the skin surface temperature elevation to be used for setting the RF safety guidelines, the frequency characteristics of the heating factors of $sIPD_s$ were investigated in this section. Figs. 7 and 8 show the heating factor of $sIPD_s$ normalized with that under plane-wave normal incidence conditions [14] as a function of the antenna–skin separation distance d normalized with λ at frequencies from 6 to 100 GHz. The data at each frequency were calculated when d was set at 2, 5, and 10 mm.

The heating factor ($\circ$C/(W/m^2)) is defined as the ratio of the local peak temperature elevation (ΔT_{peak}) at the skin surface to the spatially averaged power density [32]. This

metric was employed to estimate the local peak temperature elevation due to MMW exposure as per the safety guidelines [7]. Here, we focus on the condition that the normalized $\Delta T_{peak}/sIPD$ is significantly higher than 0 dB, where a deviation of 1 dB or more is considered as being significant, which is the same measure as that employed in the above subsections.

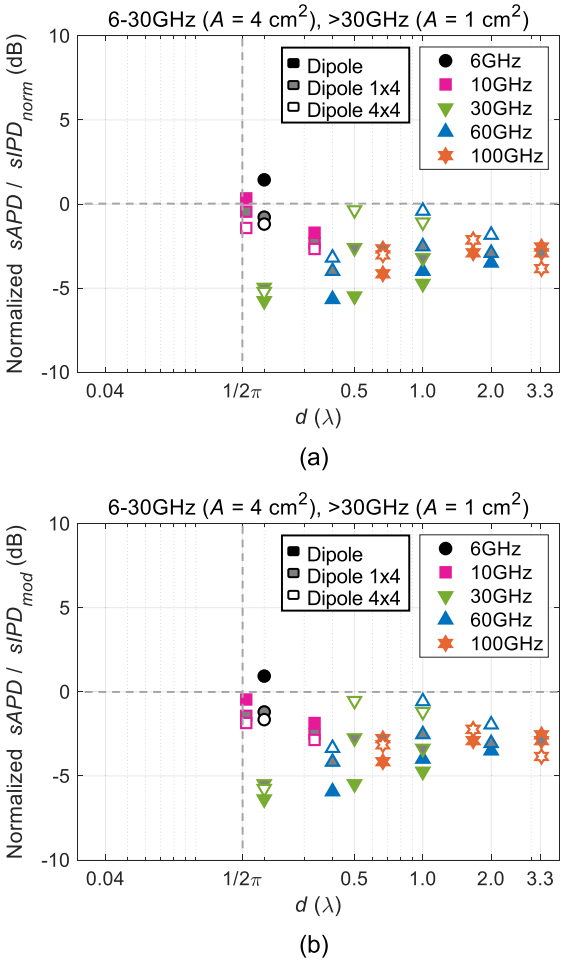

FIGURE 6. Ratios of spatially averaged absorbed to incident power densities for the dipole and dipole array antennas at frequencies from 6 to 100 GHz. The ratios are normalized with those of plane-wave normal incidence. The antenna–skin separation distances d from $\lambda/(2\pi)$ to 10 mm are normalized with the wavelength. The averaging areas are A = 4 and 1 cm^2 at or below 30 GHz and above 30 GHz, respectively: (a) $sAPD/sIPD_{norm}$, (b) $sAPD/sIPD_{mod}$.

1) DEPENDENCE ON EXPOSURE CONDITIONS

In Figs. 7 and 8, the results of $\Delta T_{peak}/sIPD$ normalized with those of the plane-wave normal incidence markedly increase when $d < \lambda/(2\pi)$, where for many cases, the deviation significantly exceeds 0 dB (> 1 dB). When $d > \lambda/(2\pi)$, depending on the exposure conditions (antenna type, frequency) and exposure evaluation methods (*sIPD* definition, averaging area), the normalized $\Delta T_{peak}/sIPD$ still exceeds 1 dB in certain cases.

The $\Delta T_{peak}/sIPD$ profiles fluctuate with the separation distance d, which tends to be minimal near $d = \lambda/(2\pi)$ and maximal close to $d = 0.1\lambda$ and $d = \lambda$. Moreover, $\Delta T_{peak}/sIPD$ normalized with that of the plane-wave incidence greatly exceeds 0 dB (> 1 dB) in the entire frequency band from 6 to 100 GHz examined in this study.

Furthermore, due to the different antenna types, a large discrepancy is observed under the condition that the normalized $\Delta T_{peak}/sIPD$ significantly exceeds 0 dB (> 1 dB), as described below. For the case of the single dipole, the normalized $\Delta T_{peak}/sIPD$ significantly exceeds 0 dB (> 1 dB) only at frequencies of 60 and 100 GHz at $d = 2$ or 5 mm. In Figs. 7 and 8, at $d < \lambda/(2\pi)$, the variation in the normalized $\Delta T_{peak}/sIPD$ among the different antenna types is relatively large (up to 11 dB). When $d > \lambda/(2\pi)$, on the other hand, the difference in the normalized $\Delta T_{peak}/sIPD$ among the antenna types is relatively small (< 6 dB).

2) DEPENDENCE ON EXPOSURE ASSESSMENT METHOD

In Figs. 7 and 8, there is no large difference in the conditions under which the normalized $\Delta T_{peak}/sIPD$ significantly exceeds 0 dB (> 1 dB) between the definitions of $sIPD_s$. The normalized $\Delta T_{peak}/sIPD_{norm}$ from plane-wave incidence is higher than that of $\Delta T_{peak}/sIPD_{mod}$. At $d < \lambda/(2\pi)$, the variation in the normalized $\Delta T_{peak}/sIPD$ due to the difference in the definition of *sIPD* is relatively large (up to 3 to 4 dB). At $d > \lambda/(2\pi)$, the corresponding variation reduces to < 1 dB.

At $d < \lambda/(2\pi)$, there is no clear difference in the conditions under which the normalized $\Delta T_{peak}/sIPD$ significantly exceeds 0 dB (> 1 dB) between the spatial averaging areas. When $d > \lambda/(2\pi)$, however, the dependence on the spatial averaging area under the considered conditions is observed. In particular, when the spatial averaging area of $A = 4$ cm^2 is employed, the normalized $\Delta T_{peak}/sIPD$ exceeds 0 dB (> 1 dB) in many cases, and this tendency is noteworthy for the array antennas. In Figs. 7 and 8, the normalized $\Delta T_{peak}/sIPD$ values with the averaging area of $A = 4$ cm^2 are relatively higher than those with $A = 1$ cm^2. In addition, it can be observed that the variations in the normalized $\Delta T_{peak}/sIPD$ due to the difference in the spatial averaging area at $d < \lambda/(2\pi)$ (up to 2.4 to 3.8 dB) are relatively smaller than those at $d > \lambda/(2\pi)$ (up to 4.4 to 5.8 dB).

3) WORST CASE

Fig. 9 shows the heating factor of $sIPD_s$ normalized with that of plane-wave normal incidence as a function of the separation distance d under the applicable conditions of $sIPD_s$ specified in the ICNIRP-2020 safety guidelines ($d \geq \lambda/(2\pi)$, $A = 4$ cm^2 at 6–30 GHz, whereas $A = 1$ cm^2 over 30 GHz).

As shown in Fig. 9, although the maximum value of the normalized $\Delta T_{peak}/sIPD_{norm}$ is smaller than the highest deviation under all the exposure scenarios, it may still significantly exceed 0 dB in some cases, e.g., 3.5 dB for the 4 × 4 dipole array at 30 GHz when $A = 4$ cm^2.

IV. DISCUSSION

In the previous section, the computational results were compared to clarify the relationships between *A*) $sIPD_{norm}$

and $sIPD_{mod}$, *B*) $sAPD/sIPD_{norm}$ and $sAPD/sIPD_{mod}$, and *C*)$\Delta T_{peak}/sIPD_{norm}$ and $\Delta T_{peak}/sIPD_{mod}$ using the four-layer skin model exposed to various antennas at near-fields. We will next further discuss our results in terms of these three relationships.

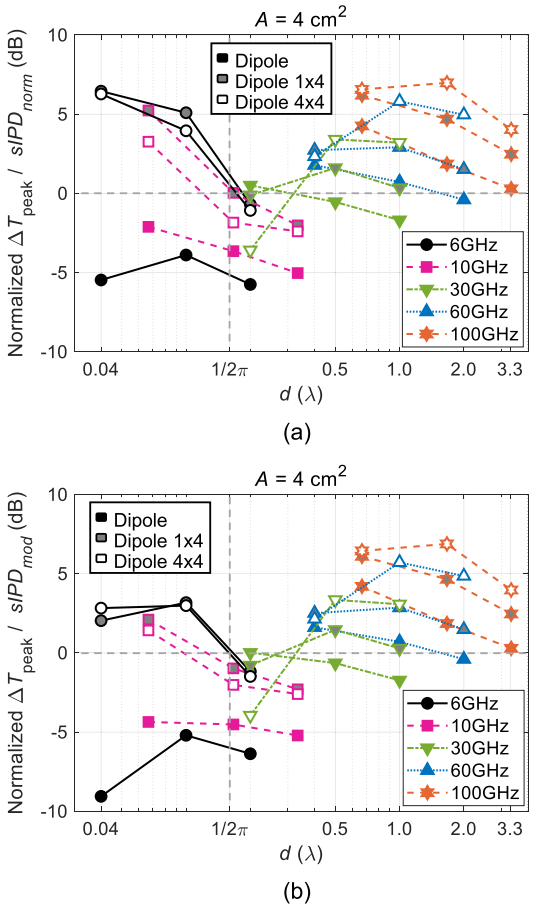

FIGURE 7. Heating factors of $sIPD_s$ for the dipole and dipole array antennas at frequencies from 6 to 100 GHz at the antenna–skin separation distances d of 2, 5, and 10 mm normalized with the wavelength in free space at each frequency when the averaging area is $A = 4$ cm^2: (a) $\Delta T_{peak}/sIPD_{norm}$, (b) $\Delta T_{peak}/sIPD_{mod}$.

A. DISCUSSION ON $sIPD_{norm}/sIPD_{mod}$

It was shown that $sIPD_{norm}/sIPD_{mod}$ is highly dependent on the distance normalized with the wavelength. The difference between $sIPD_{norm}$ and $sIPD_{mod}$ decreases monotonically with decreasing distance from the antenna and may be much lower than 0 dB (< -1 dB). At $d < \lambda/(2\pi)$, the absolute difference between $sIPD_{mod}$ and $sIPD_{norm}$ is up to 4.4 dB. This finding indicates that at the antenna near-field, $sIPD_{norm}$ may underestimate the reference level of $sIPD_{mod}$ as the metric specified in the ICNIRP-2020 safety guidelines [7]. These results correspond well with the conclusion reported in [25]. However, in the applicable range of $sIPD_s$ specified in the RF safety guidelines ($d \geq \lambda/(2\pi)$), as shown in Fig. 3, the lowest value of $sIPD_{norm}/sIPD_{mod}$ is within -1 dB. This value is not significant compared with the uncertainty due to the thickness and dielectric constants of body parts (about 1 dB) reported in [13] and the reduction factor of 2 (about 3 dB) for the exposure limits considered in the guidelines [7]. Therefore, the impact of underestimating $sIPD_{mod}$ by using $sIPD_{norm}$ on the exposure compliance assessment is not significant for the conditions assumed in this study.

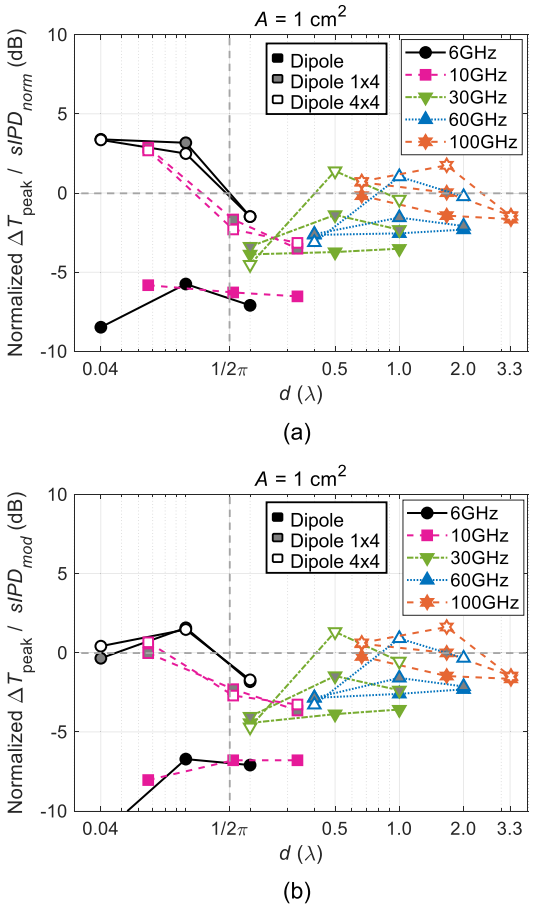

FIGURE 8. Heating factors of $sIPD_s$ for the dipole and dipole array antennas at frequencies from 6 to 100 GHz at the antenna–skin separation distances d of 2, 5, and 10 mm normalized with the wavelength in free space at each frequency when the averaging area is $A = 1$ cm^2: (a) $\Delta T_{peak}/sIPD_{norm}$, (b) $\Delta T_{peak}/sIPD_{mod}$.

It is also noted that the ICNIRP-2020 safety guidelines use $d = \lambda/(2\pi)$ as a rough guide of the boundary between the reactive and radiative near-fields, which means that more appropriate boundary conditions should be used for individual antennas. Therefore, we examined other reactive near-field boundary conditions, as described below:

1. For a linear dipole antenna, the boundary condition is slightly extended from $\lambda/(2\pi)$ to $0.62\sqrt{D^3/\lambda}$ [40], e.g., the distance for a half-wavelength dipole is 0.22λ, where D denotes the antenna length.
2. For a linear/planar array antenna, the boundary between the reactive and radiative near-field regions is related to the antenna's geometrical size, but it can be approximated to λ when the maximum dimension of the antenna is less than 2.5λ [43].

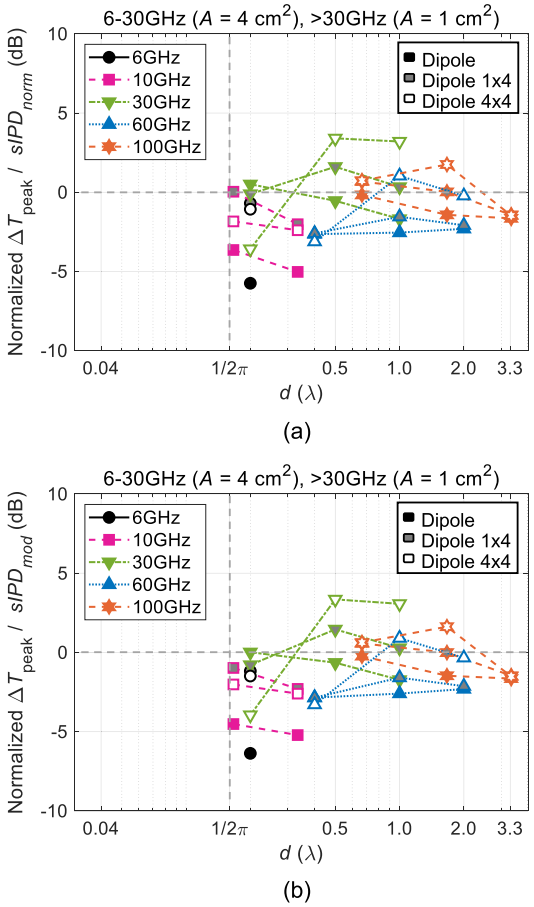

FIGURE 9. Heating factors of $sIPD_s$ for the dipole and dipole array antennas at frequencies from 6 to 100 GHz normalized with the wavelength in free space at each frequency. The antenna–skin separation distances d from $\lambda/(2\pi)$ to 10 mm are normalized with the wavelength. The averaging areas are $A = 4$ and 1 cm^2 at or below 30 GHz and above 30 GHz, respectively: (a) $\Delta T_{peak}/sIPD_{norm}$, (b) $\Delta T_{peak}/sIPD_{mod}$.

From the above consideration, we apply the boundary conditions of $d < 0.62\sqrt{D^3/\lambda}$ for the single dipole antenna and $d < \lambda$ for the 1×4 and 4×4 dipole array antennas. It is shown that when employing the above individual reactive near-field boundary conditions, the lowest $sIPD_{norm}/sIPD_{mod}$ is -0.5 dB under the conditions of applying the guidelines. Therefore, the underestimation of $sIPD_{mod}$ by $sIPD_{norm}$ can be further improved when using more appropriate boundary conditions between the reactive and radiative antenna near-fields.

B. DISCUSSION ON THE NORMALIZED sAPD/sIPD

The ratio of *sAPD* to *sIPD* normalized with that of the plane-wave incidence is also highly dependent on the distance normalized with the wavelength. The ratio of *sAPD* to *sIPD* markedly increases (above 1 dB) with decreasing antenna–skin separation distance d in several cases. This indicates that in the vicinity of the antenna, even if *sIPD* is lower than the reference level, *sAPD* can exceed the basic restrictions. However, from the results in Sec. III. B, we observed that the maximum deviations of the ratios of *sAPD* to *sIPD* for the near-fields from those of plane-wave normal incidence are 1.4 dB and 0.9 dB for $sIPD_{norm}$ and $sIPD_{mod}$, respectively. These observations are in reasonable agreement with those in [25], where a deviation of about 2 dB (1.6 times) from the plane-wave equivalent transmission at distances $d > \lambda/(2\pi)$ is reported. Consequently, in consideration of the uncertainty evaluation reported in [13] and the reduction factor of 2 (about 3 dB) for the exposure limits used in safety guidelines [7], the impact of this degree of deviation is not significant.

On the other hand, when the reactive near-field boundary conditions for individual antennas in the discussion of $sIPD_{norm}/sIPD_{mod}$ are employed, both $sAPD/sIPD_{norm}$ and $sAPD/sIPD_{mod}$ are less than 0 dB under the applicable conditions specified in the safety guidelines. Therefore, the underestimation of *sAPD* can also be ignored when using appropriate boundary conditions of the reactive near-field.

C. DISCUSSION ON THE NORMALIZED $\Delta T_{peak}/sIPD$

The ratio of ΔT_{peak} to *sIPD* normalized with that of plane-wave incidence is highly dependent on the separation distance normalized with the wavelength and the utilized antenna type. The normalized $\Delta T_{peak}/sIPD$ significantly exceeds 0 dB (>1 dB) in some cases. This indicates that even if *sIPD* is lower than the reference level, ΔT_{peak} may exceed the exposure level derived from the operational health effect threshold with the reduction factors employed in the RF safety guidelines, e.g., 0.5°C in a general public environment. Similar to the discussion of *sAPD*/*sIPD*, the ratio of ΔT_{peak} to *sIPD* for plane-wave incidence exposures was used as the rationale for setting the basic restriction (*sAPD*) and reference levels (*sIPD*) derived from *sAPD* in the safety guidelines. Thus, if the normalized $\Delta T_{peak}/sIPD$ significantly exceeds 0 dB (>1 dB), then ΔT_{peak} may exceed the exposure level considering the operational health effect threshold with the reduction factors.

From the results in Sec. III. C, we observed that the highest deviations of the ratios of ΔT_{peak} to *sIPD* for $sIPD_{norm}$ and $sIPD_{mod}$ from those of plane-wave normal incidence under the applicable conditions of $sIPD_s$ specified in the guidelines are 3.5 dB and 3.3 dB, respectively. These values are comparable to the uncertainty reported in [13] and the reduction factor considered in the safety guidelines [7]. Therefore, the impact of underestimating ΔT_{peak} by $sIPD_{norm}$ and $sIPD_{mod}$ (and perhaps *sAPD*) on the safety compliance assessment may not be negligible.

When the reactive near-field boundary conditions for the individual antennas are applied, the maximum deviations of the normalized $\Delta T_{peak}/sIPD_{norm}$ and $\Delta T_{peak}/sIPD_{mod}$ under the applicable conditions of $sIPD_s$ specified in the safety guidelines are still significant, i.e., 3.2 dB and 3.1 dB, respectively. Therefore, it may not be possible to improve the underestimation of ΔT_{peak} by using more appropriate reactive near-field boundary conditions.

In the ICNIRP-2020 safety guidelines, the spatial averaging area of 1 cm^2 is applied above 30 GHz but not at

30 GHz. Because an ideal beam can be focused within one wavelength, the beam width of the antenna may be narrow compared with 4 cm^2 (2 cm × 2 cm) at or below 30 GHz. Therefore, it may be necessary to employ the averaging area of 1 cm^2 at lower frequencies (for example, above 15 GHz where the wavelength is 2 cm). It is shown that when applying the spatial averaging area of 1 cm^2 at 30 GHz (4 cm^2 so far) in addition to the reactive near-field boundary conditions of the individual antennas, the highest normalized $\Delta T_{peak}/sIPD_{norm}$ and $\Delta T_{peak}/sIPD_{mod}$ reduce to 1.7 and 1.6 dB, respectively. Therefore, the impact of underestimating ΔT_{peak} may be reduced when employing the spatial averaging area of 1 cm^2 at frequencies of 30 GHz or lower. This suggests that a suitable area for spatial averaging lies in the range between 1 and 4 cm^2, as pointed out in [35].

Furthermore, we only observed a normalized $\Delta T_{peak}/sIPD$ of over 3 dB under the applicable conditions in the current RF safety guidelines in the case of 4 × 4 dipole arrays. For the other antennas with smaller dimensions, the highest values under the applicable conditions in the current RF safety guidelines were 1.5 to 1.6 dB for the cases of $\Delta T_{peak}/sIPD_{norm}$ and $\Delta T_{peak}/sIPD_{mod}$. Note that 4 × 4 antenna arrays are relatively large and may not be suitable for installation in the existing 5G user equipment operating at 28 GHz. Thus, the current guidelines may still protect a human body from EMF exposure from 5G terminals mounted with an ordinary four-element array antenna.

V. CONCLUSION

In this study, we investigated the spatially averaged power densities for localized exposure to EMFs at MMW frequencies. Two spatially averaged $sIPD_s$ in the safety guidelines and standards, i.e., $sIPD_{norm}$ and $sIPD_{mod}$, were compared via a computational evaluation approach. Their relationships with each other, s*APD*, and the local peak temperature elevation at the skin surface were analyzed using three types of antennas at distances of 2 to 10 mm from the skin surface at frequencies ranging from 6 to 100 GHz.

The investigations demonstrated that outside the typical boundary of the reactive near-field, i.e., $> \lambda/(2\pi)$, which is used as a rough guide of the applicable condition for reference levels in the RF safety guidelines, but at most 10 mm from the antennas, the maximum difference between $sIPD_{norm}$ and $sIPD_{mod}$ is at most 0.7 dB. For the appropriate conditions recommended in the RF safety guidelines, the differences between the ratios of *sAPD* to *sIPD* and the ratio for the normal incidence of plane-wave exposures are at most 1.4 dB and 0.9 dB for $sIPD_{norm}$ and $sIPD_{mod}$, respectively. Furthermore, we found that for the appropriate conditions recommended in the RF safety guidelines, the heating factors of $sIPD_s$ for the relatively small antennas (i.e., the dipole and 1 × 4 dipole array, for both of which the total dimension is smaller than 2λ) do not significantly exceed those for the plane-wave normal incidence, which means that the expected maximum temperature elevation is lower than the operational health effect threshold in terms of the temperature elevation with the reduction factors employed in the RF safety guidelines. It is, however, shown that for the other cases with the large antenna (4 × 4 dipole array, whose total dimension is larger than 2λ), the ratios can increase up to 3.5 dB and 3.3 dB for $sIPD_{norm}$ and $sIPD_{mod}$, respectively, from those for the plane-wave normal incidence.

These results provide suggestive evidence that the effect of the definition of $sIPD_s$ on the human exposure characteristics is not significant compared with those of other factors, such as the antenna type (size), frequency, distance from the radiation source, and spatial averaging area. The findings of this study are useful for discussing the appropriate definition of $sIPD_s$ for the safety guidelines and their compliance procedures in cases of near-field exposure conditions above 6 GHz.

REFERENCES

[1] M. Zhadobov, N. Chahat, R. Sauleau, C. Le Quement, and Y. Le Drean, "Millimeter-wave interactions with the human body: State of knowledge and recent advances," *Int. J. Microw. Wireless Technol.*, vol. 3, no. 2, pp. 237–247, 2011.
[2] T. Wu, T. S. Rappaport, and C. M. Collins, "Safe for generations to come: Considerations of safety for millimeter waves in wireless communications," *IEEE Microw. Mag.*, vol. 16, no. 2, pp. 65–84, Mar. 2015.
[3] A. R. Guraliuc, M. Zhadobov, R. Sauleau, L. Marnat, and L. Dussopt, "Near-field user exposure in forthcoming 5G scenarios in the 60 GHz band," *IEEE Trans. Antennas Propag.*, vol. 65, no. 12, pp. 6606–6615, Dec. 2017.
[4] M. C. Ziskin, S. I. Alekseev, K. R. Foster, and Q. Balzano, "Tissue models for RF exposure evaluation at frequencies above 6 GHz," *Bioelectromagnetics*, vol. 39, no. 3, pp. 173–189, Apr. 2018.
[5] A. Hirata, "Review on human dosimetry for radio-frequency exposure above 6 GHz-international exposure standards," in *Proc. Asia–Pacific Microw. Conf. (APMC)*, Nov. 2018, pp. 681–683.
[6] A. Hirata, D. Funahashi, and S. Kodera, "Setting exposure guidelines and product safety standards for radio-frequency exposure at frequencies above 6 GHz: Brief review," *Ann. Telecommun.*, vol. 74, nos. 1–2, pp. 17–24, Feb. 2019.
[7] International Commission on Non-Ionizing Radiation Protection (ICNIRP), "Guidelines for limiting exposure to time-varying electric, magnetic and electromagnetic fields (100 kHz to 300 GHz)," *Health Phys.*, vol. 118, no. 5, pp. 483–524, May 2020.
[8] *IEEE Standard for Safety Levels With Respect to Human Exposure to Radio Frequency Electromagnetic Fields, 0 Hz to 300 GHz*, IEEE Standard C95.1-2019, New York, NY, USA, 2019.
[9] *Measurement Procedure for the Evaluation of Power Density Related to Human Exposure to Radio Frequency Fields From Wireless Communication Devices Operating Between 6 GHz and 100 GHz*, IEC document TC106-63170, Aug. 2018.
[10] S. I. Alekseev, A. A. Radzievsky, M. K. Logani, and M. C. Ziskin, "Millimeter wave dosimetry of human skin," *Bioelectromagnetics*, vol. 29, no. 1, pp. 65–70, Jan. 2008.
[11] A. Kanezaki, A. Hirata, S. Watanabe, and H. Shirai, "Effects of dielectric permittivities on skin heating due to millimeter wave exposure," *Biomed. Eng. OnLine*, vol. 8, no. 1, p. 20, 2009.
[12] A. Kanezaki, A. Hirata, S. Watanabe, and H. Shirai, "Parameter variation effects on temperature elevation in a steady-state, one-dimensional thermal model for millimeter wave exposure of one-and three-layer human tissue," *Phys. Med. Biol.*, vol. 55, no. 16, pp. 4647–4659, Jul. 2010.
[13] K. Sasaki, M. Mizuno, K. Wake, and S. Watanabe, "Monte Carlo simulations of skin exposure to electromagnetic field from 10 GHz to 1 THz," *Phys. Med. Biol.*, vol. 62, no. 17, pp. 6993–7010, Aug. 2017.
[14] K. Li, K. Sasaki, S. Watanabe, and H. Shirai, "Relationship between power density and surface temperature elevation for human skin exposure to electromagnetic waves with oblique incidence angle from 6 GHz to 1 THz," *Phys. Med. Biol.*, vol. 64, no. 6, Mar. 2019, Art. no. 065016.

[15] A. Christ, T. Samaras, E. Neufeld, and N. Kuster, "RF-induced temperature increase in a stratified model of the skin for plane-wave exposure at 6–100 GHz," *Radiat. Protection Dosimetry*, vol. 188, no. 3, pp. 350–360, Mar. 2020.
[16] B. Thors, D. Colombi, Z. Ying, T. Bolin, and C. Törnevik, "Exposure to RF EMF from array antennas in 5G mobile communication equipment," *IEEE Access*, vol. 4, pp. 7469–7478, 2016.
[17] K. Foster and D. Colombi, "Thermal response of tissue to RF exposure from canonical dipoles at frequencies for future mobile communication systems," *Electron. Lett.*, vol. 53, no. 5, pp. 360–362, Mar. 2017.
[18] W. He, B. Xu, M. Gustafsson, Z. Ying, and S. He, "RF compliance study of temperature elevation in human head model around 28 GHz for 5G user equipment application: Simulation analysis," *IEEE Access*, vol. 6, pp. 830–838, 2018.
[19] W. He, B. Xu, Y. Yao, D. Colombi, Z. Ying, and S. He, "Implications of incident power density limits on power and EIRP levels of 5G millimeter-wave user equipment," *IEEE Access*, vol. 8, pp. 148214–148225, Aug. 2020.
[20] B. Xu, K. Zhao, B. Thors, D. Colombi, O. Lundberg, Z. Ying, and S. He, "Power density measurements at 15 GHz for RF EMF compliance assessments of 5G user equipment," *IEEE Trans. Antennas Propag.*, vol. 65, no. 12, pp. 6584–6595, Dec. 2017.
[21] B. Xu, K. Zhao, Z. Ying, D. Sjöberg, W. He, and S. He, "Analysis of impacts of expected RF EMF exposure restrictions on peak EIRP of 5G user equipment at 28 GHz and 39 GHz bands," *IEEE Access*, vol. 7, pp. 20996–21005, 2019.
[22] E. Carrasco, D. Colombi, K. R. Foster, M. Ziskin, and Q. Balzano, "Exposure assessment of portable wireless devices above 6 GHz," *Radiat. Prot. Dosim.*, vol. 183, no. 4, pp. 489–496, Jun. 2019.
[23] D. Colombi, B. Thors, C. TöRnevik, and Q. Balzano, "RF energy absorption by biological tissues in close proximity to mmW 5G wireless equipment," *IEEE Access*, vol. 6, pp. 4974–4981, 2018.
[24] T. Nakae, D. Funahashi, J. Higashiyama, T. Onishi, and A. Hirata, "Skin temperature elevation for incident power densities from dipole arrays at 28 GHz," *IEEE Access*, vol. 8, pp. 26863–26871, Jan. 2020.
[25] A. Christ, T. Samaras, E. Neufeld, and N. Kuster, "Limitations of incident power density as a proxy for induced electromagnetic fields," *Bioelectromagnetics*, vol. 41, no. 5, pp. 348–359, May 2020.
[26] K. Sasaki, K. Wake, and S. Watanabe, "Measurement of the dielectric properties of the epidermis and dermis at frequencies from 0.5 GHz to 110 GHz," *Phys. Med. Biol.*, vol. 59, no. 16, pp. 4739–4747, Aug. 2014.
[27] A. Taflove and S. C. Hagness, *Computational Electrodynamics: The Finite-Difference Time-Domain Method*, 3rd ed. Norwood, MA, USA: Artech House, 2005.
[28] K. Sasaki, T. Sakai, T. Nagaoka, K. Wake, S. Watanabe, M. Kojima, N. Hasanova, H. Sasaki, K. Sasaki, Y. Suzuki, M. Taki, Y. Kamimura, A. Hirata, and H. Shirai, "Dosimetry using a localized exposure system in the millimeter-wave band for *in vivo* studies on ocular effects," *IEEE Trans. Microw. Theory Techn.*, vol. 62, no. 7, pp. 1554–1564, Jul. 2014.
[29] A. Hirata and O. Fujiwara, "The correlation between mass-averaged SAR and temperature elevation in the human head model exposed to RF near-fields from 1 to 6 GHz," *Phys. Med. Biol.*, vol. 54, no. 23, pp. 7227–7238, Dec. 2009.
[30] R. Morimoto, I. Laakso, V. De Santis, and A. Hirata, "Relationship between peak spatial-averaged specific absorption rate and peak temperature elevation in human head in frequency range of 1–30 GHz," *Phys. Med. Biol.*, vol. 61, no. 14, pp. 5406–5425, Jul. 2016.
[31] R. Morimoto, A. Hirata, I. Laakso, M. C. Ziskin, and K. R. Foster, "Time constants for temperature elevation in human models exposed to dipole antennas and beams in the frequency range from 1 to 30 GHz," *Phys. Med. Biol.*, vol. 62, no. 5, pp. 1676–1699, Feb. 2017.
[32] Y. Hashimoto, A. Hirata, R. Morimoto, S. Aonuma, I. Laakso, K. Jokela, and K. R. Foster, "On the averaging area for incident power density for human exposure limits at frequencies over 6 GHz," *Phys. Med. Biol.*, vol. 62, no. 8, pp. 3124–3138, Apr. 2017.
[33] H. H. Pennes, "Analysis of tissue and arterial blood temperatures in the resting human forearm," *J. Appl. Physiol.*, vol. 1, no. 2, pp. 93–122, 1948.
[34] K. R. Foster, A. Lozano-Nieto, P. J. Riu, and T. S. Ely, "Heating of tissues by microwaves: A model analysis," *Bioelectromagnetics*, vol. 19, no. 7, pp. 420–428, 1998.
[35] K. R. Foster, M. C. Ziskin, and Q. Balzano, "Thermal modeling for the next generation of radiofrequency exposure limits: Commentary," *Health Phys.*, vol. 113, no. 1, pp. 41–53, 2017.
[36] D. Funahashi, T. Ito, A. Hirata, T. Iyama, and T. Onishi, "Averaging area of incident power density for human exposure from patch antenna arrays," *IEICE Trans. Electron.*, vol. E101.C, no. 8, pp. 644–646, Aug. 2018.
[37] A. Hirata, S. Kodera, K. Sasaki, J. Gomez-Tames, I. Laakso, A. Wood, S. Watanabe, and K. R. Foster, "Human exposure to radiofrequency energy above 6 GHz: Review of computational dosimetry studies," *Phys. Med. Biol.*, vol. 66, no. 8, Apr. 2021, Art. no. 08TR01.
[38] A. Hirata, I. Laakso, T. Oizumi, R. Hanatani, K. H. Chan, and J. Wiart, "The relationship between specific absorption rate and temperature elevation in anatomically based human body models for plane wave exposure from 30 MHz to 6 GHz," *Phys. Med. Biol.*, vol. 58, no. 4, pp. 903–921, 2013.
[39] A. Hirata, M. Fujimoto, T. Asano, J. Wang, O. Fujiwara, and T. Shiozawa, "Correlation between maximum temperature increase and peak SAR with different average schemes and masses," *IEEE Trans. Electromagn. Compat.*, vol. 48, no. 3, pp. 569–578, Aug. 2006.
[40] C. A. Balanis, "Antenna theory," in *Analysis and Design*, 3rd ed. Hoboken, NJ, USA: Wiley, 2005, pp. 34–35.
[41] D. Funahashi, A. Hirata, S. Kodera, and K. R. Foster, "Area-averaged transmitted power density at skin surface as metric to estimate surface temperature elevation," *IEEE Access*, vol. 6, pp. 77665–77674, 2018.
[42] Y. Diao, E. A. Rashed, and A. Hirata, "Assessment of absorbed power density and temperature rise for nonplanar body model under electromagnetic exposure above 6 GHz," *Phys. Med. Biol.*, vol. 65, no. 22, Nov. 2020, Art. no. 224001.
[43] I. T. I. S. 62232, *Determination of RF Field Strength, Power Density and SAR in the Vicinity of Radiocommunication Base Stations for the Purpose of Evaluating Human Exposure*, IEC TC106 International Standard 62232, Aug. 2017.

KUN LI (Member, IEEE) received the B.E. degree in communication engineering from Nanjing University of Posts and Telecommunications, Nanjing, China, in 2011, and the M.E. and Ph.D. degrees in electrical engineering from Toyama University, Toyama, Japan, in 2014 and 2017, respectively.

From 2017 to 2019, he was a Researcher with the Electromagnetic Compatibility Laboratory, National Institute of Information and Communications Technology (NICT), Tokyo, Japan. He is currently an Assistant Professor at Kagawa University, Japan. His research interests include bio-EMC issues on EMF safety, over-the-air testing for MIMO, and body area network systems.

Dr. Li is a member of IEICE. He was a recipient of the IEEE AP-S Japan Student Award, in 2015, the IEICE Best Letter Award, in 2017, Risaburo Sato Award of EMC Sapporo & AMPEC, in 2019, and the Young Scientist Award of the URSI, in 2020.

KENSUKE SASAKI (Member, IEEE) received the B.E., M.E., and Ph.D. degrees in electrical and electronic engineering from Tokyo Metropolitan University, Tokyo, Japan, in 2006, 2008, and 2011, respectively.

He is currently with the National Institute of Information and Communications Technology (NICT), Tokyo. His research interests include electromagnetic theory, bioelectromagnetics, and dielectric properties measurement.

Dr. Sasaki was a member of the Scientific Expert Group of International Commission on Non-Ionizing Radiation Protection (ICNIRP), from 2018 to 2020. He has been the Early Carrier Representative of Commission K, the International Scientific Radio Union (URSI), since 2017. He was a recipient of the 2009 Young Scientist Award of the URSI, the 2012 Best Paper Award of the IEEJ, and the 2020 Achievement Award of the IEICE.

KANAKO WAKE (Member, IEEE) received the B.E., M.E., and D.E. degrees in electrical engineering from Tokyo Metropolitan University, Tokyo, Japan, in 1995, 1997, and 2000, respectively.

She is currently with the National Institute of Information and Communications Technology, Tokyo, where she is involved in research on biomedical electromagnetic compatibility.

Dr. Wake is a member of the Institute of Electronics, Information and Communication Engineers, the Institute of Electrical Engineers, Japan, and the Bioelectromagnetics Society. She was a recipient of the 1999 International Scientific Radio Union Young Scientist Award.

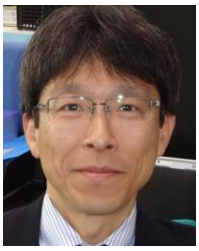

TERUO ONISHI (Member, IEEE) received the B.S. degree in physics from Tokyo University of Science, Tokyo, Japan, in 1987, and the Ph.D. degree from the Graduate School of Science and Technology, Chiba University, Chiba, Japan, in 2005.

He was with Toyo Communication Equipment Company, Ltd., Kanagawa, Japan, and Nippon Ericsson K.K., Tokyo. From 1990 to 1992, he was with Hokkaido University, Sapporo, Japan, where he was involved in the finite-difference time-domain (FDTD) analysis for solving electromagnetic problems. He was a Senior Research Engineer with NTT DOCOMO, Inc., Kanagawa, from 2002 to 2019. He was a Project Professor with Nagoya Institute of Technology, Japan, from 2014 to 2017, and a Visiting Professor with Tohoku University, Japan, in 2017. He joined the National Institute of Information and Communications Technology, Tokyo, in 2019. His current research interests include electromagnetic field (EMF) exposure measurement and the standardization of EMF evaluation method.

Dr. Onishi was a Board Member of the Bioelectromagnetics Society (BEMS), from 2016 to 2018. He was a member of the Institute of Electronics, Information, and Communication Engineers (IEICE). He received the 1906 Award from the IEC, in 2017. He was a Project Leader of IEC TC106 PT63184. He is a Chair of the IEEE International Committee on Electromagnetic Safety (ICES) TC-34 and a Convener of the International Electrotechnical Commission (IEC) TC106 JWG12.

SOICHI WATANABE (Senior Member, IEEE) received the B.E., M.E., and D.E. degrees in electrical engineering from Tokyo Metropolitan University, Tokyo, Japan, in 1991, 1993, and 1996, respectively.

He is currently with the National Institute of Information and Communications Technology, Tokyo.

Dr. Watanabe was a member of the Standing Committee III on Physics and Engineering of the International Commission on Non-Ionizing Radiation Protection (ICNIRP), from 2004 to 2012. He has been a member of the Main Commission of ICNIRP, since 2012. He is a member of the Institute of Electronics, Information and Communication Engineers, the Institute of Electrical Engineers, Japan, and the Bioelectromagnetics Society. He received the 1996 Young Scientist Award of the International Scientific Radio Union, the 1997 Best Paper Award of the IEICE, the 2004 Best Paper Award (The Roberts Prize) of Physics in Medicine and Biology, the Risaburo Sato Award of EMC Sapporo & APEMC 2019, and the 2020 Achievement Award of the IEICE.